ACS Sustainable Chemistry & Engineering

Research Article

pubs.acs.org/journal/ascecg

A General Strategy To Fabricate Ni_xP as Highly Efficient Cocatalyst via Photoreduction Deposition for Hydrogen Evolution

Yuming Dong,*[,†] Linggang Kong,[†] Pingping Jiang,[†] Guangli Wang,[†] Na Zhao,[†] Huizhen Zhang,[†] and Bo Tang*[,‡]

[†]Key Laboratory of Synthetic and Biological Colloids, School of Chemical and Material Engineering, Jiangnan University, Wuxi 214122, P. R. China

[‡]College of Chemistry, Chemical Engineering and Materials Science, Shandong Provincial Key Laboratory of Clean Production of Fine Chemicals, Collaborative Innovation Center of Functionalized Probes for Chemical Imaging in Universities of Shandong, Shandong Normal University, Jinan 250014, P. R. China

Supporting Information

ABSTRACT: Presently, precise deposition of transition metal phosphides at the electron outlet of photoactive materials as cocatalysts for hydrogen generation is rarely reported. Demonstrated here is a general photochemical strategy for the preparation of metal phosphides as cocatalysts for hydrogen generation. In this work, Ni_xP was successfully deposited on g-C_3N_4 using nickel sulfate ($NiSO_4$) and hypophosphite sodium (NaH_2PO_2) as Ni and P sources, respectively. The Ni_xP/g-C_3N_4 composite exhibits excellent performance of hydrogen evolution via water splitting (about 8585 μmol g^{-1} h^{-1} in a triethanolamine aqueous solution under a 300 W Xe lamp with an AM 1.5G filter). More importantly, due to the intrinsic acid-resistant properties of Ni_xP and g-C_3N_4, the Ni_xP/g-C_3N_4 composite demonstrated excellent acid-stable photocatalytic activity for H_2 evolution (stable run for 75 h under acidic solution of pH 2). Furthermore, the mechanism for photocatalytic activity of g-C_3N_4 enhanced by Ni_xP was investigated in detail by steady-state photoluminescence spectra and surface photovoltage spectra, which indicated that separation efficiency of photogenerated carriers from g-C_3N_4 was effectively enhanced by Ni_xP.

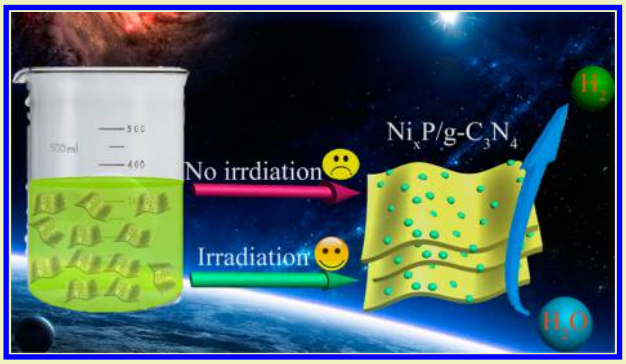

KEYWORDS: *Photocatalysis, Hydrogen generation, Photochemical, Water splitting, Metal phosphide*

INTRODUCTION

The global energy crisis and environmental pollution are becoming increasingly serious. Development of an environmentally friendly new energy is extremely urgent. The sunlight-driven generation of the energy carrier H_2 from water is considered as one of the most promising strategies.[1] As is known, the photocatalytic hydrogen evolution reaction (HER) involves absorption of light, separation of electron−hole pairs, and oxidation and reduction reactions. Because the rates of final chemical reactions are lower than those of light harvesting and charge separation, cocatalysts are always necessary for high efficiency. In photocatalytic hydrogen production, the main function of the cocatalyst is transferring photogenerated electrons to protons, and the process of charge transfer is influenced directly by the position where the cocatalyst is loaded. The connective point between the cocatalyst and photoactive materials is desirable to be located at the electron outlet points of photoactive materials. Recently, photoreduction deposition of noble metals such as Pt as an HER cocatalyst at the electron outlet has been approved by Li's group, and the precisely prepared sample revealed higher activity than those with cocatalysts randomly deposited.[2−4] Their intensive works revealed great advantage and promising application of the photoreduction route for preparation of an HER cocatalyst. At the same time, noble metals are high cost and rare, which limits large-scale applications. Therefore, expending a photoreduction deposition method to an inexpensive, robust, and stable HER cocatalyst is significant for development of a commercially available photocatalyst. Recently, many good works about non-noble or noble metals prepared by the photoreduction deposition method for photocatalysts have been reported.[5−7]

Composed of Earth-abundant elements, transition metal phosphides are low-cost compounds. In 2005, the possibility of transition metal phosphide (Ni_2P) as a highly active HER catalyst was first predicted by density functional theory calculations.[8] Then, many transition metal phosphides, such as FeP, CoP and Co_2P, Ni_2P and Ni_5P_4, CoNiP, MoP, and

Received: April 9, 2017
Revised: May 30, 2017
Published: June 8, 2017

DOI: 10.1021/acssuschemeng.7b01079
ACS Sustainable Chem. Eng. 2017, 5, 6845−6853

Cu_3P, were reported as HER electrocatalysts and revealed outstanding performance, including low overpotential and excellent durability.[9−24] Some electrodes based on metal phosphides worked well under a wide pH range of 0−14.[11−14] From 2014, transition metal (Fe, Co, Ni, and Cu) phosphides were proposed as efficient cocatalysts of CdS[25−28] or g-C_3N_4[29−32] for photocatalytic hydrogen generation. These great works indicated promising applications of transition metal phosphides as photocatalytic HER cocatalysts. However, up to now, most of the reported metal phosphides in photocatalytic systems are linked or mixed with photoactive materials randomly, and photoreduction deposition of metal phosphides as efficient cocatalysts is rarely reported.[33]

With the above background in mind, we explored the photoreduction deposition route of transition metal phosphides as cocatalysts of g-C_3N_4. A graphitic carbon nitride polymer (g-C_3N_4) has stimulated intensive research in photocatalytic water splitting since 2009, and a cocatalyst is extremely necessary to inhibit the rapid recombination of photogenerated electron−hole pairs and enhance the reduction rate of protons.[34−43] Therefore, g-C_3N_4 was chosen as the sample of photoactive material. On the basis of our recent works about photodeposition methods,[33,44,45] herein, a facile photoreduction route of Ni_xP was proposed and realized. In this process, $NiSO_4$ and NaH_2PO_2 were used, respectively, as the sources of Ni and P, and the content of Ni_xP on the surface of g-C_3N_4 can be adjusted by changing the irradiation time. Using this method, the Ni_xP nanoparticle was precisely loaded on the electron outlet points of g-C_3N_4, which is beneficial for quick transport of the photogenerated electrons. The optimized hydrogen evolution rate of Ni_xP/g-C_3N_4 was about 8585 μmol g^{-1} h^{-1} under a 300 W Xe lamp with an AM 1.5G filter. In addition, due to the intrinsic chemical properties of g-C_3N_4 and metal phosphide, the Ni_xP/g-C_3N_4 composite photocatalyst exhibits strong vitality (runs for 75 h) under acidic solution (pH 2).

EXPERIMENTAL SECTION

Chemicals. All reagents, including thiourea (99%), triethanolamine (98%), nickel sulfate hexahydrate (98.5%), sodium hypophosphite monohydrate (98%), methanol (99.5%), lactic acid (85%), sodium hydroxide (96%), and chloroplatinic acid hexahydrate (37% Pt basis), were purchased from Sinopharm Chemical Reagent Co., Ltd. and used without further purification.

Preparation of Graphitic C_3N_4 (g-C_3N_4) Nanosheets. The g-C_3N_4 nanosheets were prepared using a modified method which was reported by previous literatures.[44,45] In a typical process, 20 g of thiourea in a crucible was heated to 550 °C with a ramp rate of 2 °C min^{-1} and maintained at this temperature for 2 h in an air atmosphere. Then, the resultant yellow bulk g-C_3N_4 was milled into fine powder, placed in an open porcelain crucible, heated to 500 °C with a ramp rate of 2 °C min^{-1}, and maintained at this temperature for 2 h in an air atmosphere. Finally, light yellow powder (about 0.1 g) of g-C_3N_4 was obtained.

Photochemical Synthesis of Ni_xP/g-C_3N_4 Composite. The Ni_xP/g-C_3N_4 composite was prepared by a photochemical method. First, 30 mg of g-C_3N_4, 4.0 mL of $NiSO_4$ aqueous solution (0.10 mol L^{-1}), 4.0 mL of NaH_2PO_2 aqueous solution (0.70 mol L^{-1}), and 2 mL of H_2O were mixed in a 40 mL flask at ambient temperature. Then, the mixed system was purged by pure nitrogen for 40 min. Subsequently, the mixture was illuminated under UV−vis light (300 W Xe lamp). After illumination, the precipitates were washed with distilled water and dried under N_2 flowing. The deposition content of Ni_xP can be adjusted by changing the time of illumination. The obtained products were named as Ni_xP-T/g-C_3N_4, where T refers to the illumination time (min) under UV−vis light.

Characterization Methods. To confirm the composition and phase of the sample, X-ray diffraction (XRD) patterns were recorded on a D8 X-ray diffractometer (Bruker AXS, German). Size and lattice fringe measurements were analyzed by transmission electron microscopy (TEM) using a JEM-2100Plus transmission electron microscope (JEOL, Japan). An environmental scanning electron microscope (Hitachi S-4800) coupled with an energy-dispersive X-ray spectroscope (SEM/EDX) was also employed to investigate the microscopic features. The EDX-mapping images were obtained with a Tecnai G2 F30 transmission electron microscope (FEI, USA) equipped with a Rontec EDX system. UV−vis absorption spectra were measured using a spectrophotometer (Shimadzu, Japan UV-3600 Plus). Fourier transform infrared (FTIR) spectra were recorded over the 4000−800 cm^{-1} range using a Nicolet 6700 (Thermal, USA) infrared spectrometer with a DLaTGS detector. Raman spectra were recorded on a confocal microscopic Raman spectrometer (Renishow InVia, USA) with a 785 nm laser light irradiation from 200 to 2000 cm^{-1} at a duration time of 10 s. The X-ray photoelectron spectroscopy (XPS) analysis was conducted using an ESCALAB 250 Xi (Thermo, USA) X-ray photoelectron spectrometer with Al Kα as the excitation source ($h\nu$ = 1484.6 eV). Photoluminescence (PL) measurements were carried out on a CARY Eclipse (Varian, USA) fluorescence spectrophotometer. The surface photovoltage (SPV) was determined for investigating charges features by a self-made equipment.[45] Electrochemistry measurements were performed by a CHI660E electrochemical analyzer (Chenhua Instruments Co., China), with an Ag/AgCl electrode used as the reference electrode, Pt wire employed as the counter electrode, and glassy carbon electrode as the working electrode.

Photocatalytic Hydrogen Production. In photocatalytic HER experiments, an Ni_xP-T/g-C_3N_4 composite photocatalyst was first added to water containing a sacrificial agent in a 40 mL flask. Then, the mixture was treated by sonication for 5 min and purged by pure nitrogen gas for 40 min. Finally, the system was irradiated under a light source for certain time at ambient temperature, and a 300 W Xe lamp with an AM 1.5G filter (average optical power density 95 mW cm^{-2}) was employed as the light source. The generated hydrogen was measured by gas chromatography (FULI GC9790 using a 5 Å molecular sieve column, argon as a carrier gas) with a thermal conductivity detector (TCD). Detailed amounts of photocatalysts and compositions of aqueous solutions are given in the captions of the corresponding figures.

RESULTS AND DISCUSSION

First, control experiments were designed to investigate the influence of the preparation time (irradiation time under light) of Ni_xP/g-C_3N_4 on the photocatalytic HER activity. The photocatalytic HER data in 20 vol % triethanolamine aqueous solution are shown in Figure S1. Due to the fast recombination of photogenerated carriers, the photocatalytic H_2 evolution rate of the Ni_xP-0/g-C_3N_4 sample was only 27 μmol g^{-1} h^{-1}, which is very low. With Ni_xP loaded on the surface of g-C_3N_4, the photocatalytic HER activity was increased obviously. The HER activity was about 6310 μmol g^{-1} h^{-1} for Ni_xP-10/g-C_3N_4, and the highest photocatalytic activity of 8585 μmol g^{-1} h^{-1} was achieved using Ni_xP-20/g-C_3N_4 as the photocatalyst. We can find that the photocatalytic HER activity of Ni_xP-20/g-C_3N_4 was about 318 times higher than that of pure g-C_3N_4. The results demonstrate that Ni_xP was an effective cocatalyst for g-C_3N_4. However, when the preparation time was prolonged further, the photocatalytic activity revealed a slight decrease. For example, the photocatalytic activity of Ni_xP-30/g-C_3N_4 was 7269 μmol g^{-1} h^{-1} and that of Ni_xP-40/g-C_3N_4 was 6381 μmol g^{-1} h^{-1}. When methanol and lactate acid were used as hole scavengers (Figure S2), Ni_xP-20/g-C_3N_4 also revealed the

DOI: 10.1021/acssuschemeng.7b01079
ACS Sustainable Chem. Eng. 2017, 5, 6845−6853

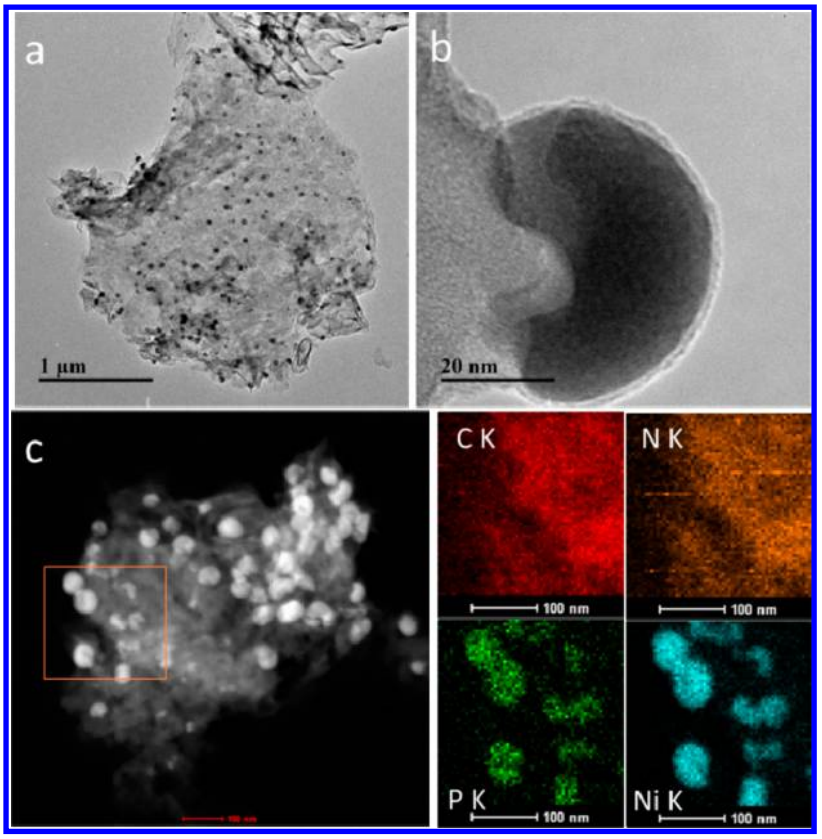

Figure 1. (a, b) TEM image and (c) EDX-mapping image of Ni_xP-20/g-C_3N_4.

highest HER activity among the Ni_xP-T/g-C_3N_4 samples (T = 0, 10, 20, and 30 min). This phenomenon can be explained that, as an effective cocatalyst, Ni_xP on a g-C_3N_4 surface can also impede the incident light absorption of g-C_3N_4. Obviously, there is an optimum irradiation time in the preparation process, and 20 min was proper for preparation of a Ni_xP/g-C_3N_4 composite. Therefore, the photochemical preparation time of Ni_xP/g-C_3N_4 was set as 20 min, and the Ni_xP-20/g-C_3N_4 sample was widely used in the next experiments.

According to the reported results summarized in Table S1, Ni_xP-20/g-C_3N_4 behaved with higher efficiency and is among the most robust HER photocatalysts composed of g-C_3N_4 and non-noble-metal cocatalysts. For comparison, we measured the HER activity of Ni_xP-20/g-C_3N_4 and 0.5 wt % Pt/g-C_3N_4 under the same conditions as shown in Figure S3. Moreover, the TEM and HRTEM images of Pt-0.5 wt %/g-C_3N_4 are shown in Figure S4. The content of Pt is about 0.43 wt % in the sample of Pt-0.5 wt %/g-C_3N_4 according to the result of ICP-MS. The photocatalytic H_2 evolution rate of 0.5 wt % Pt/g-C_3N_4 was about 10114 μmol g^{-1} h^{-1}, which was higher than that of Ni_xP-20/g-C_3N_4 (8585 μmol g^{-1} h^{-1}). Because Ni_xP/g-C_3N_4 is made of Earth-abundant elements, Ni_xP can serve as an important substitute of precious platinum for photocatalytic H_2 production.

Characterization of Ni_xP/g-C_3N_4. Figure S5a shows the XRD pattern of Ni_xP-T/g-C_3N_4 (T = 0, 10, 20, 30, 40, and 100). Two feature diffraction peaks at around 27.4° and 13.0° of g-C_3N_4 (JCPDS 87-1526) appeared in all samples, which indicated that the structural features of g-C_3N_4 were unchanged during the synthesis of Ni_xP. The intensity of the broad peak between 40° and 50° was slightly enhanced with the increase in irradiation time. However, there was no obvious diffraction peak of Ni_xP for all samples, even with the irradiation time prolonged to 100 min. These results indicate the amorphous structure of obtained Ni_xP. The FTIR spectra (Figure S5b) and Raman spectra (Figure S6) were obtained to investigate the molecular structure of Ni_xP-T/g-C_3N_4. The broad IR peak between 3000 and 3300 cm^{-1} corresponded to uncondensed terminal amino groups and O−H bands of surface-absorbed H_2O molecules. A broad IR absorption band appeared between 900 and 1800 cm^{-1}, which corresponded to the polycondensation structure of g-C_3N_4.[46] The FTIR spectra of all Ni_xP-T/g-C_3N_4 samples showed nearly identical absorption bands, indicating that the molecular structure of the g-C_3N_4 nanosheet was unchanged after the introduction of Ni_xP. For all the samples, two feature Raman bands at around 1300 and 1500 cm^{-1}, respectively, related to the disordered D and graphitic G,[39] and the Raman peaks in the region between 600 and 800 cm^{-1} should be due to the in-plane rotation of 6-fold rings in a graphitic carbon nitride layer.[47] The results also indicated that the loading of Ni_xP did not change the structure of g-C_3N_4. However, the intensity of the Raman peak of g-C_3N_4 reduced gradually with the increase in irradiation time, which illustrated that Ni_xP on the surface of g-C_3N_4 inhibited the photons to g-C_3N_4 to a certain extent.

The light-absorption performances of Ni_xP-T/g-C_3N_4 (T = 10, 20, 30, 40, and 100) were investigated by UV−vis-diffuse reflectance spectra, which is shown in Figure S7. According to these results, the absorption edge of the pure g-C_3N_4 was about 450 nm, which corresponded to a band gap of 2.75 eV. When Ni_xP was introduced, the light absorption in the visible region of Ni_xP-T/g-C_3N_4 was obviously enhanced, and the results are coincident with the color of these samples (insert, Figure S7).

DOI: 10.1021/acssuschemeng.7b01079
ACS Sustainable Chem. Eng. 2017, 5, 6845−6853

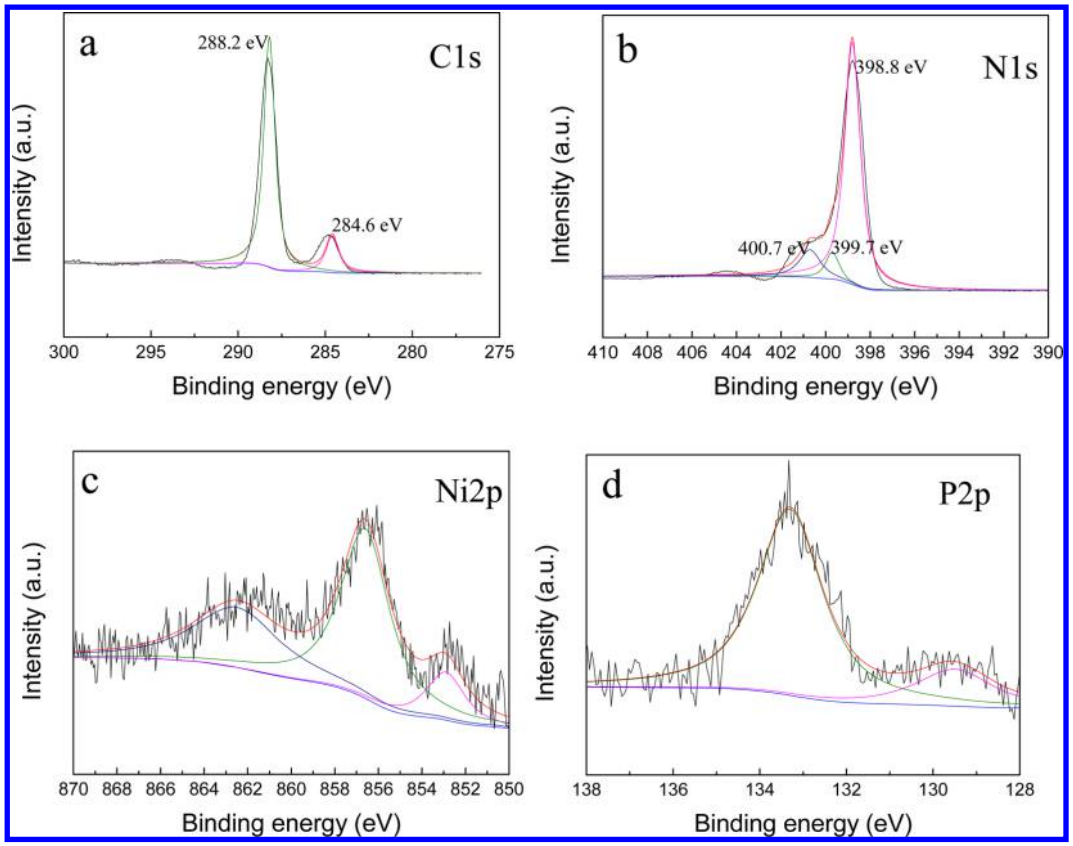

Figure 2. High-resolution XPS spectra of Ni_xP-20/g-C_3N_4: (a) C 1s, (b) N 1s, (c) Ni 2p, and (d) P 2p.

TEM and SEM were used to observe the morphology of Ni_xP-20/g-C_3N_4, and the results are given in Figure 1 and Figure S8. Ni_xP nanoparticles with an average size of about 40 nm were tightly deposited on the surface of g-C_3N_4 nanosheets. To further determine the elements distribution, the elemental mapping analysis was carried out. Energy-dispersive X-ray (EDX) elemental mapping images of C, N, P, and Ni for Ni_xP-20/g-C_3N_4 are shown in Figure 1c. Both Ni and P elements are uniformly distributed throughout these nanoparticles, while both C and N elements are uniformly distributed throughout on nanosheets. The distributional ranges of C/N and Ni/P were excellently overlapped. The weight content of Ni and P in Ni_xP-20/g-C_3N_4 were determined as 4.263% and 0.970% by SEM/EDX, and the ratio of Ni to P was calculated as 2.341.

The composition and chemical status of C, N, P, and Ni for Ni_xP-20/g-C_3N_4 were investigated by X-ray photoelectron spectroscopy (XPS). As shown in Figure 2a, the peak at 284.6 and 288.2 eV in the high-resolution C 1s spectrum can be ascribed to the C−C/C═C and O−C═O groups, respectively.[48] The N 1s XPS peak (Figure 2b) can be fitted into three peaks corresponding to sp2-hybridized nitrogen (C═N−C) at 398.8 eV, tertiary nitrogen ($N(C)_3$) at 399.7 eV, and amino functional groups at 400.7 eV, respectively.[41] The binding energies of C 1S and N 1S were matched with that of g-C_3N_4. The peaks of Ni 2p (Figure 2c) appeared at 852.9 and 856.7 eV. The peak at 852.9 eV was attributed to $Ni^{\delta+}$ in the Ni_xP phase.[9,14,32] For P 2p (Figure 2d), the peak at 129.5 eV was attributed to $P^{\delta-}$ in the Ni_xP phase.[14,28,32] Moreover, the peak at 856.7 eV of Ni 2p ascribed to Ni^{2+} formed by surface oxidation due to air contact.[29] The peak at 133.1 eV of P 2p was assigned to P−O species from surface oxidation.[32,49] The broad peak at 862.5 eV should be the Ni 2p satellite peak.[32] There was no metallic Ni detected in the high-resolution XPS spectra of Ni 2p. The results of XPS spectra indicated that Ni_xP was obtained by photochemical strategy.

Preparation Conditions of Ni_xP. Then, control experiments were carried out to investigate the effect of various conditions on the photochemical formation of Ni_xP. The experimental conditions were set as shown in Table 1.

Table 1. Preparation Conditions for Control Experiments

	g-C_3N_4/mg	$NiSO_4$ (0.1M)/mL	NaH_2PO_2 (0.7M)/mL	H_2O/mL	irradiation/min
A	30	4	4	2	20
B	30	4	–	6	20
C	30	–	4	6	20
D	30	4	4	2	dark 20
E	0	4	4	2	20

Experiment A is the typical preparation of Ni_xP-20/g-C_3N_4, including g-C_3N_4, $NiSO_4$, NaH_2PO_2, and irradiation for 20 min under UV−vis light. In experiment B, the mixture including g-C_3N_4 and $NiSO_4$ was treated for 20 min under UV−vis light, and the difference from experiment A is the absence of NaH_2PO_2. In experiment C, the mixture including g-C_3N_4 and NaH_2PO_2 was treated for 20 min under UV−vis light, and the difference from experiment A is the absence of $NiSO_4$. In experiment D, the same mixture as that in experiment A was treated under dark (without irradiation of light) for 20 min. In experiment E, the mixture including $NiSO_4$ and NaH_2PO_2 was treated for 20 min under UV−vis light, and the difference from experiment A is the absence of g-C_3N_4. After 20 min of treatment, the solid samples from A, B, C, and D were washed

DOI: 10.1021/acssuschemeng.7b01079
ACS Sustainable Chem. Eng. 2017, 5, 6845−6853

and dried according to the same procedure as Ni_xP-20/g-C_3N_4. No solid was observed and obtained from experiment E, indicating the unique role of photoactive material. Then, the photocatalytic hydrogen evolution activity of the solid obtained from experiments A, B, C, and D were tested, and the HER activity data were shown in Figure 3. It can be found that the

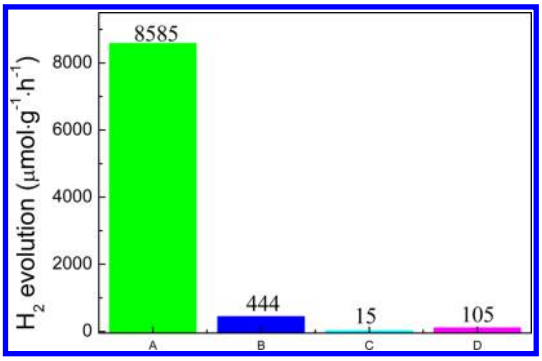

Figure 3. Comparison of the photocatalytic H_2 evolution activity of samples A, B, C, and D obtained by control experiments in Table 1. The data were obtained by photocatalytic processes of 5 mg of photocatalyst in 10 mL 20 vol % triethanolamine aqueous solution for 2 h.

HER activity of sample A (8585 μmol g^{-1} h^{-1}) was much higher than that of samples B (444 μmol g^{-1} h^{-1}), C (15 μmol g^{-1} h^{-1}), and D (105 μmol g^{-1} h^{-1}). Therefore, for the photosynthesis of efficient cocatalyst Ni_xP, all of photoactive material (such as g-C_3N_4), nickel salt (such as $NiSO_4$), proper phosphorus source hypophosphites (such as NaH_2PO_2), and irradiation are essential and necessary.

As is known, with the middle valence state of phosphorus, hypophosphites reveal reduction performance and oxidation property at the same time. For instance, NaH_2PO_2 can undergo thermal decomposition to P(-III) and P(+V) at elevated temperatures about 300−400 °C. Under irradiation, the photoactive material (such as g-C_3N_4) adsorbed light and produced hole−electron pairs. The photogenerated electrons and holes were subsequently transported to the surface. Under this condition, parts of $H_2PO_2^-$ were reduced by the electrons and others were oxidized by the holes.

Are the electrons on conductive band (CB) of g-C_3N_4 proper for the above reactions? In order to prove the feasibility of the above reactions, the current−potential curve (J-V) of the clear solution (without g-C_3N_4) in experiments A, B, and C were investigated. From Figure 4, the reduction potential of pure Ni^{2+} was determined as −0.993 V vs NHE and that of pure $H_2PO_2^-$ was −0.818 V vs NHE. When Ni^{2+} and $H_2PO_2^-$ were mixed, the reduction potential moved to −0.734 V vs NHE. The results indicated that, although both Ni^{2+} and $H_2PO_2^-$ can be reduced under certain potential, the formation of Ni_xP was prior. The conclusion is coincident with the photochemical reaction results in Table 1. The results were also coincident with the electrochemical preparation of metal phosphide by the reduction process (cobalt phosphide).[21] Furthermore, the reduction potential of the mixture of Ni^{2+} and $H_2PO_2^-$ match well with CB of g-C_3N_4.

Acid-Stable Photocatalytic HER Performance of Ni_xP/g-C_3N_4. Most of the currently reported photocatalytic HER systems are unstable under acidic conditions due to the intrinsic chemical properties of photocatalysts themselves. For example, when CdS materials were used as the photoactive material for

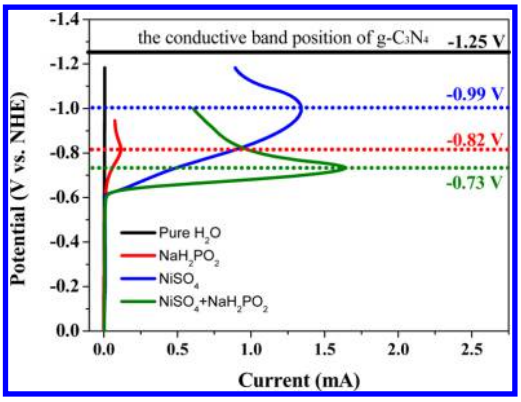

Figure 4. Current−potential curve (J-V) of pure H_2O and the clear solution (without g-C_3N_4) in experiments A, B, and C according to Table 1. Glassy carbon electrode was used as the working electrode, and all scanning rates were 0.1 V/s.

hydrogen generation in the presence of lactic acid, the reaction rate decreased gradually due to the decomposition of CdS.[26,27] From the view of practical applications, development of an efficient, commercially available, and acid-stable photocatalyst is necessary and significant. In fact, good acid stability of a photocatalyst means durability of the cocatalyst as well as the photoactive material in acidic aqueous solutions.

Ni_xP-20/g-C_3N_4 is very desirable as an efficient, commercially available, and acid-stable photocatalyst. Then, in order to investigate the photocatalytic HER performance in acid conditions, 10 vol % lactic acid aqueous solution (pH 2.0) was used as a sacrificial agent. As shown in Figure 5a, during the long-time experiment of 75 h, no obvious decrease in the hydrogen production rate was observed along with an increase in photocatalytic time. The total amount of H_2 within 75 h was about 115 mmol g^{-1}, and the average HER activity was calculated as 1533 μmol g^{-1} h^{-1}. In addition, the cycling runs of the photocatalytic HER experiment of Ni_xP-20/g-C_3N_4 were carried out. As shown in Figure 5b, in the experiment of 24 h, there was no decrease in the HER activity through each cycles. These results indicate that Ni_xP-20/g-C_3N_4 is an acid-stable photocatalyst with excellent activity.

In addition, another experiment was carried out to investigate the acid stability. Ni_xP-20/g-C_3N_4 was dispersed in an HCl solution (0.01 M, pH 2.0) for 1 week, and then, the sample was washed with distilled water and dried. The photocatalytic HER activity of Ni_xP-20/g-C_3N_4 after the above treatment was determined, and there was not any decrease in activity. Furthermore, according to the TEM image (Figure S9) and EDX-mapping image (Figure S10), no obvious changes in morphology and composition were observed. These results also indicate that Ni_xP-20/g-C_3N_4 is stable in acidic conditions.

Mechanism for Enhanced HER Activity by Ni_xP. Compared with pure g-C_3N_4, Ni_xP/g-C_3N_4 revealed stronger absorption for visible light (Figure S7). Is the enhanced absorption of visible light responsible for the remarkable photocatalytic activity of Ni_xP-20/g-C_3N_4? A control experiment was designed, and the results are shown in Figure 6. The photocatalytic activity of H_2 evolution along with wavelength coincided well with the UV−vis absorption spectrum of pure g-C_3N_4, not that of Ni_xP-20/g-C_3N_4. The results indicated that the enhanced absorption in the visible region from Ni_xP hardly contributed to the high photocatalytic activity of Ni_xP-20/g-

DOI: 10.1021/acssuschemeng.7b01079
ACS Sustainable Chem. Eng. 2017, 5, 6845−6853

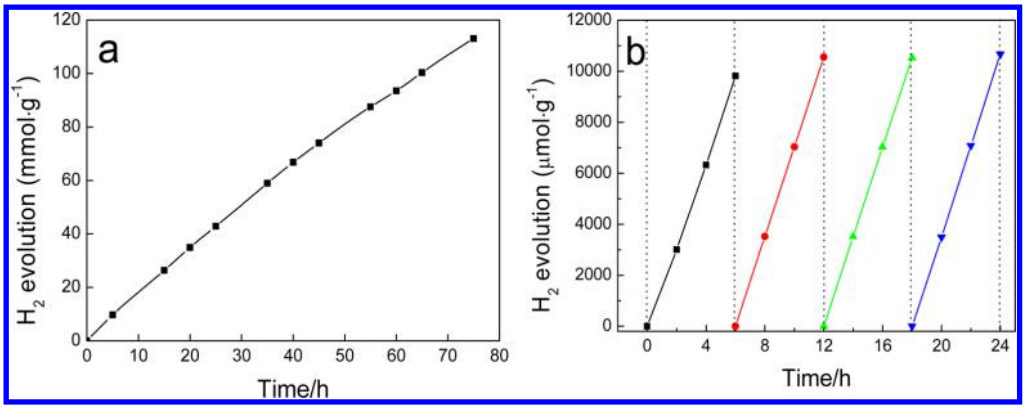

Figure 5. (a) Long-time photocatalytic H_2 evolution of Ni_xP-20/g-C_3N_4. (b) Cycling runs for photocatalytic hydrogen evolution of Ni_xP-20/g-C_3N_4. The produced H_2 was evacuated every 6 h. Both systems contained 5 mg of Ni_xP-20/g-C_3N_4 in 10 mL of 10 vol % lactic acid aqueous solution.

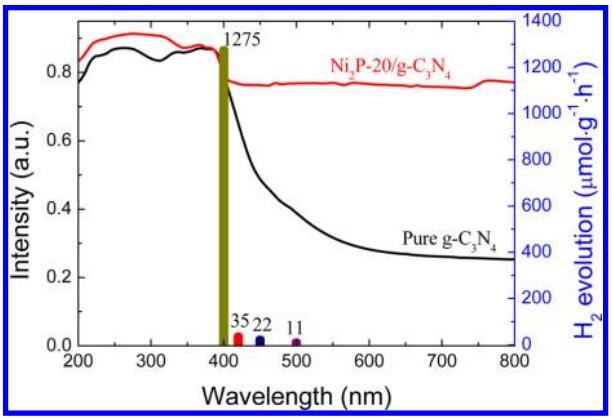

Figure 6. UV−vis-diffuse reflectance spectra of pure g-C_3N_4 and Ni_xP-20/g-C_3N_4 and the H_2 evolution rate of Ni_xP-20/g-C_3N_4 along with light wavelength. The photocatalytic system contained 5 mg of Ni_xP-20/g-C_3N_4 in 10 mL of 20 vol % triethanolamine aqueous solution, and a 300 W Xe lamp with a different band-pass filter was used as the light source.

C_3N_4. The results well demonstrated the cocatalyst role of Ni_xP in this hybrid photocatalyst.

The improved photocatalytic activity for hydrogen evolution was probably due to the fast interfacial transfer of photogenerated electron−hole pairs between g-C_3N_4 and Ni_xP. The PL spectra of pure g-C_3N_4 and Ni_xP-20/g-C_3N_4 was investigated, which is able to reflect the transfer of photogenerated charge carriers. As shown in Figure 7a, both pure g-C_3N_4 and Ni_xP-20/g-C_3N_4 showed distinct emission bands at about 450 nm under an excitation wavelength of 325 nm. However, the PL intensity of Ni_xP-20/g-C_3N_4 was much weaker than that of pure g-C_3N_4. The results suggested that the charge recombination of g-C_3N_4 was effectively suppressed by loading of Ni_xP.[30,31]

In order to further study the mechanism, the surface photovoltages (SPV) of pure g-C_3N_4 and Ni_xP-20/g-C_3N_4 were determined. As shown in Figure 7b, both pure g-C_3N_4 and Ni_xP-20/g-C_3N_4 revealed obvious positive photovoltage responses in the range from 300 to 400 nm, which match well with the photoactive wavelength range of not Ni_xP but g-C_3N_4. These results indicated that the band gap of g-C_3N_4 was not changed after loading of Ni_xP, and the results further supported the conclusion obtained from Figure 6. Moreover, the photovoltage intensity of Ni_xP-20/g-C_3N_4 was much higher than that of pure g-C_3N_4. It has been reported that a stronger photoelectric signal means higher charge separation efficiency.[50] The results indicated that separation efficiency of photogenerated carriers from g-C_3N_4 was effectively enhanced by Ni_xP.

As shown in Figure 8, the schematic of the photocatalytic H_2 evolution mechanism for the Ni_xP/g-C_3N_4 heterostructures system was proposed. Under the irradiation of light, electron−hole pairs generate from g-C_3N_4. However, the photogenerated electrons and holes easily recombine in the absence of a cocatalyst. After loading Ni_xP on the surface of g-C_3N_4, the

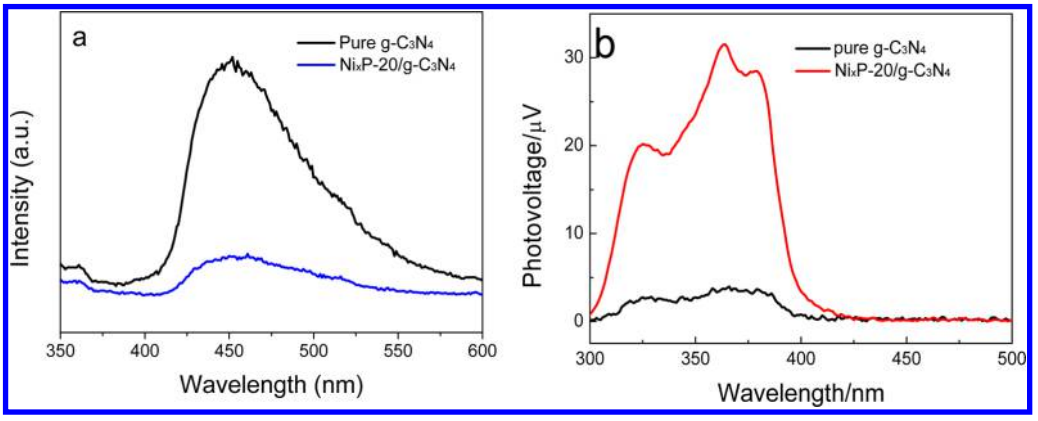

Figure 7. (a) Photoluminescence (PL) spectra of pure g-C_3N_4 and Ni_xP-20/g-C_3N_4 under excitation wavelength of 325 nm. (b) Surface photovoltage (SPV) of pure g-C_3N_4 and Ni_xP-20/g-C_3N_4.

DOI: 10.1021/acssuschemeng.7b01079
ACS Sustainable Chem. Eng. 2017, 5, 6845−6853

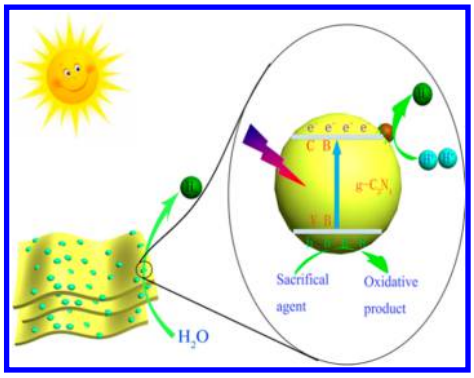

Figure 8. Proposed photocatalytic H_2 production mechanism schematic of $Ni_xP/g\text{-}C_3N_4$ composite.

photogenerated electrons in the conduction band of $g\text{-}C_3N_4$ can easily transfer to Ni_xP and then easily be consumed by H^+. Therefore, the photocatalytic HER activity of $g\text{-}C_3N_4$ was enhanced greatly by the deposition of Ni_xP.

CONCLUSIONS

In this work, a photochemical strategy was proposed for the preparation of metal phosphides as cocatalysts of $g\text{-}C_3N_4$ for the first time, and Ni_xP was successfully deposited on electron outlet points of $g\text{-}C_3N_4$ by the photochemical route. For the photosynthesis of Ni_xP, photoactive material (such as $g\text{-}C_3N_4$), nickel salt (such as $NiSO_4$), a proper phosphorus source hypophosphites (such as NaH_2PO_2), and irradiation are necessary. Because the separation efficiency of photogenerated carriers from $g\text{-}C_3N_4$ was effectively enhanced by Ni_xP, the $Ni_xP/g\text{-}C_3N_4$ composite acts as one of the most robust HER photocatalysts composed of $g\text{-}C_3N_4$ and non-noble-metal cocatalysts. Due to the intrinsic chemical properties of Ni_xP and $g\text{-}C_3N_4$, the $Ni_xP/g\text{-}C_3N_4$ composite demonstrated excellent acid-stable photocatalytic activity for H_2 evolution, which has been a challenging function up to now. Because $Ni_xP/g\text{-}C_3N_4$ is made of Earth-abundant elements, this opens a door for development of an efficient, commercially available, and acid-stable HER photocatalyst.

ASSOCIATED CONTENT

Supporting Information

The Supporting Information is available free of charge on the ACS Publications website at DOI: 10.1021/acssuschemeng.7b01079.

Table S1: Photocatalytic H_2 evolution on $g\text{-}C_3N_4$ with non-noble-metal cocatalysts. Table S2: Photocatalytic H_2 evolution from water using lactic acid as hole sacrificial agent. Figures S1 and S2: Photocatalytic HER activity of $Ni_xP\text{-}T/g\text{-}C_3N_4$. Figure S3: Photocatalytic HER activity of Pt-0.5 wt %/$g\text{-}C_3N_4$. Figure S4: TEM (left) and HRTEM (right) image of Pt-0.5 wt %/$g\text{-}C_3N_4$. Figures S5–S8: XRD pattern, FTIR spectra, Raman spectra, UV–vis diffuse reflectance spectra, and SEM image of $Ni_xP\text{-}T/g\text{-}C_3N_4$. Figures S9 and S10: TEM image and EDX-mapping image of Ni-20/$g\text{-}C_3N_4$ after treatment in HCl solution (pH 2) for 1 week. Figure S11: Property and function of AM 1.5G filter. (PDF)

AUTHOR INFORMATION

Corresponding Authors

*Yuming Dong. E-mail: dongym@jiangnan.edu.cn. Fax: +86 510 85917763.

*Bo Tang. E-mail: tangb@sdnu.edu.cn.

ORCID

Yuming Dong: 0000-0002-2999-1325

Bo Tang: 0000-0002-8712-7025

Author Contributions

The manuscript was written through contributions of all authors. All authors have given approval to the final version of the manuscript.

Notes

The authors declare no competing financial interest.

ACKNOWLEDGMENTS

The authors gratefully acknowledge the support from the National Natural Science Foundation of China (No. 21676123, 21575052), Natural Science Foundation of Jiangsu Province (No. BK20161127), Fundamental Research Funds for the Central Universities (JUSRP51623A), Opening Foundation of Shandong Provincial Key Laboratory of Clean Production of Fine Chemicals (ZDSYS-KF201504) from Shandong Normal University, and MOE & SAFEA for the 111 Project (B13025). The authors also thank Dr. Jinze Lv for his kind help on SPV technology.

REFERENCES

(1) Liu, J.; Liu, Y.; Liu, N.; Han, Y.; Zhang, X.; Huang, H.; Lifshitz, Y.; Lee, S.; Zhong, J.; Kang, Z. Metal-free efficient photocatalyst for stable visible water splitting *via* a two-electron pathway. *Science* **2015**, *347*, 970–974.

(2) Zhu, J.; Fan, F.; Chen, R.; An, H.; Feng, Z.; Li, C. Direct Imaging of Highly Anisotropic Photogenerated Charge Separations on Different Facets of a Single $BiVO_4$ Photocatalyst. *Angew. Chem.* **2015**, *127*, 9239–9242.

(3) Li, R.; Zhang, F.; Wang, D.; Yang, J.; Li, M.; Zhu, J.; Zhou, X.; Han, H.; Li, C. Spatial separation of photogenerated electrons and holes among {010} and {110} crystal facets of $BiVO_4$. *Nat. Commun.* **2013**, *4*, 1432–1438.

(4) Mu, L.; Zhao, Y.; Li, A.; Wang, S.; Wang, Z.; Yang, J.; Liu, T.; Chen, R.; Zhu, J.; Fan, F.; Li, R.; Li, C.; Wang, Y. Enhancing charge separation on high symmetry $SrTiO_3$ exposed with anisotropic facets for photocatalytic water splitting. *Energy Environ. Sci.* **2016**, *9*, 2463–2469.

(5) Li, Y.; Wang, H.; Peng, S. Tunable photodeposition of MoS_2 onto a composite of reduced graphene oxide and CdS for synergic photocatalytic hydrogen generation. *J. Phys. Chem. C* **2014**, *118*, 19842–19848.

(6) Xu, J.; Li, Y.; Peng, S. Photocatalytic hydrogen evolution over Erythrosin B-sensitized graphitic carbon nitride with in situ grown molybdenum sulfide cocatalyst. *Int. J. Hydrogen Energy* **2015**, *40*, 353–362.

(7) Li, Y.; Hou, Y.; Fu, Q.; Peng, S.; Hu, Y. Oriented growth of $ZnIn_2S_4/In(OH)_3$ heterojunction by a facile hydrothermal transformation for efficient photocatalytic H_2 production. *Appl. Catal., B* **2017**, *206*, 726–733.

(8) Liu, P.; Rodriguez, J. A. Catalysts for hydrogen evolution from the [NiFe] hydrogenase to the Ni_2P (001) surface: the importance of ensemble effect. *J. Am. Chem. Soc.* **2005**, *127*, 14871–14878.

(9) Kibsgaard, J.; Tsai, C.; Chan, K.; Benck, J. D.; Nørskov, J. K.; Abild-Pedersen, F.; Jaramillo, T. F. Designing an improved transition metal phosphide catalyst for hydrogen evolution using experimental and theoretical trends. *Energy Environ. Sci.* **2015**, *8*, 3022–3029.

DOI: 10.1021/acssuschemeng.7b01079
ACS Sustainable Chem. Eng. 2017, 5, 6845–6853

(10) Shi, Y.; Zhang, B. Recent advances in transition metal phosphide nanomaterials: synthesis and applications in hydrogen evolution reaction. *Chem. Soc. Rev.* **2016**, *45*, 1529−1541.
(11) Tian, J.; Liu, Q.; Asiri, A. M.; Sun, X. Self-supported nanoporous cobalt phosphide nanowire arrays: an efficient 3D hydrogen-evolving cathode over the wide range of pH 0−14. *J. Am. Chem. Soc.* **2014**, *136*, 7587−7590.
(12) Laursen, A. B.; Patraju, K. R.; Whitaker, M. J.; Retuerto, M.; Sarkar, T.; Yao, N.; Ramanujachary, K. V.; Greenblatt, M.; Dismukes, G. C. Nanocrystalline Ni_5P_4: a hydrogen evolution electrocatalyst of exceptional efficiency in both alkaline and acidic media. *Energy Environ. Sci.* **2015**, *8*, 1027−1034.
(13) Han, A.; Chen, H.; Zhang, H.; Sun, Z.; Du, P. Ternary Metal Phosphide Nanosheets as Highly Efficient Electrocatalyst for Water Reduction to Hydrogen over a Wide pH Range from 0 to 14. *J. Mater. Chem. A* **2016**, *4*, 10195−10202.
(14) Shi, Y.; Xu, Y.; Zhuo, S.; Zhang, J.; Zhang, B. Ni_2P nanosheets/Ni foam composite electrode for long-lived and pH-tolerable electrochemical hydrogen generation. *ACS Appl. Mater. Interfaces* **2015**, *7*, 2376−2384.
(15) Xu, Y.; Wu, R.; Zhang, J.; Shi, Y.; Zhang, B. Anion-exchange synthesis of nanoporous FeP nanosheets as electrocatalysts for hydrogen evolution reaction. *Chem. Commun.* **2013**, *49*, 6656−6658.
(16) Popczun, E. J.; Read, C. G.; Roske, C. W.; Lewis, N. S.; Schaak, R. E. Highly active electrocatalysis of the hydrogen evolution reaction by cobalt phosphide nanoparticles. *Angew. Chem.* **2014**, *126*, 5531−5534.
(17) Callejas, J. F.; McEnaney, J. M.; Read, C. G.; Crompton, J. C.; Biacchi, A. J.; Popczun, E. J.; Gordon, T. R.; Lewis, N. S.; Schaak, R. E. Electrocatalytic and photocatalytic hydrogen production from acidic and neutral-pH aqueous solutions using iron phosphide nanoparticles. *ACS Nano* **2014**, *8*, 11101−11107.
(18) Huang, Z.; Chen, Z.; Chen, Z.; Lv, C.; Humphrey, M. G.; Zhang, C. Cobalt phosphide nanorods as an efficient electrocatalyst for the hydrogen evolution reaction. *Nano Energy* **2014**, *9*, 373−382.
(19) Liu, Q.; Tian, J.; Cui, W.; Jiang, P.; Cheng, N.; Asiri, A. M.; Sun, X. Carbon Nanotubes Decorated with CoP Nanocrystals: A Highly Active Non-Noble-Metal Nanohybrid Electrocatalyst for Hydrogen Evolution. *Angew. Chem.* **2014**, *126*, 6828−6832.
(20) Popczun, E. J.; McKone, J. R.; Read, C. G.; Biacchi, A. J.; Wiltrout, A. M.; Lewis, N. S.; Schaak, R. E. Nanostructured nickel phosphide as an electrocatalyst for the hydrogen evolution reaction. *J. Am. Chem. Soc.* **2013**, *135*, 9267−9270.
(21) Saadi, F. H.; Carim, A. I.; Verlage, E.; Hemminger, J. C.; Lewis, N. S.; Soriaga, M. P. CoP as an acid-stable active electrocatalyst for the hydrogen-evolution reaction: Electrochemical synthesis, interfacial characterization and performance evaluation. *J. Phys. Chem. C* **2014**, *118*, 29294−29300.
(22) Wang, X.; Kolen'ko, Y. V.; Liu, L. Direct solvothermal phosphorization of nickel foam to fabricate integrated Ni_2P-nanorods/Ni electrodes for efficient electrocatalytic hydrogen evolution. *Chem. Commun.* **2015**, *51*, 6738−6741.
(23) Xing, Z.; Liu, Q.; Asiri, A. M.; Sun, X. Closely interconnected network of molybdenum phosphide nanoparticles: a highly efficient electrocatalyst for generating hydrogen from water. *Adv. Mater.* **2014**, *26*, 5702−5707.
(24) Tian, J.; Liu, Q.; Cheng, N.; Asiri, A. M.; Sun, X. Self-Supported Cu_3P Nanowire Arrays as an Integrated High-Performance Three-Dimensional Cathode for Generating Hydrogen from Water. *Angew. Chem., Int. Ed.* **2014**, *53*, 9577−9581.
(25) Cao, S.; Chen, Y.; Wang, C. J.; He, P.; Fu, W. F. Highly efficient photocatalytic hydrogen evolution by nickel phosphide nanoparticles from aqueous solution. *Chem. Commun.* **2014**, *50*, 10427−10429.
(26) Cao, S.; Chen, Y.; Wang, C. J.; Lv, X. J.; Fu, W. F. Spectacular photocatalytic hydrogen evolution using metal-phosphide/CdS hybrid catalysts under sunlight irradiation. *Chem. Commun.* **2015**, *51*, 8708−8711.
(27) Cheng, H.; Lv, X. J.; Cao, S.; Zhao, Z. Y.; Chen, Y.; Fu, W. F. Robustly photogenerating H_2 in water using FeP/CdS catalyst under solar irradiation. *Sci. Rep.* **2016**, *6*, 19846−19855.
(28) Sun, Z.; Zheng, H.; Li, J.; Du, P. Extraordinarily efficient photocatalytic hydrogen evolution in water using semiconductor nanorods integrated with crystalline Ni_2P cocatalysts. *Energy Environ. Sci.* **2015**, *8*, 2668−2676.
(29) Chen, Y.; Qin, Z. General applicability of nanocrystalline Ni_2P as a noble-metal-free cocatalyst to boost photocatalytic hydrogen generation. *Catal. Sci. Technol.* **2016**, *6*, 8212−8221.
(30) Zhao, H.; Jiang, P.; Cai, W. CoP cocatalyst decorated graphitic C_3N_4 with enhanced and stable photocatalytic H_2 evolution activity from water under visible light irradiation. *Chem. - Asian J.* **2017**, *12*, 361.
(31) Zhao, H.; Sun, S.; Jiang, P.; Xu, Z. J. Graphitic C_3N_4 modified by Ni_2P cocatalyst: An efficient, robust and low cost photocatalyst for visible-light-driven H_2 evolution from water. *Chem. Eng. J.* **2017**, *315*, 296−303.
(32) Indra, A.; Acharjya, A.; Menezes, P. W.; Merschjann, C.; Hollmann, D.; Schwarze, M.; Aktas, M.; Friedrich, A.; Lochbrunner, S.; Thomas, A.; Driess, M. Boosting visible-light-driven photocatalytic hydrogen evolution with an integrated nickel phosphide-carbon nitride system. *Angew. Chem., Int. Ed.* **2017**, *56*, 1653−1657.
(33) Dong, Y.; Kong, L.; Wang, G.; Jiang, P.; Zhao, N.; Zhang, H. Photochemical synthesis of Co_xP as cocatalyst for boosting photocatalytic H_2 production via spatial charge separation. *Appl. Catal., B* **2017**, *211*, 245−251.
(34) Wang, X.; Maeda, K.; Thomas, A.; Takanabe, K.; Xin, G.; Carlsson, J. M.; Domen, K.; Antonietti, M. A metal-free polymeric photocatalyst for hydrogen production from water under visible light. *Nat. Mater.* **2009**, *8*, 76−80.
(35) Zheng, Y.; Lin, L.; Wang, B.; Wang, X. Graphitic carbon nitride polymers toward sustainable photoredox catalysis. *Angew. Chem., Int. Ed.* **2015**, *54*, 12868−12884.
(36) Gong, Y.; Li, M.; Wang, Y. Carbon nitride in energy conversion and storage: Recent advances and future prospects. *ChemSusChem* **2015**, *8*, 931−946.
(37) Yin, S.; Han, J.; Zhou, T.; Xu, R. Recent progress in g-C_3N_4 based low cost photocatalytic system: activity enhancement and emerging applications. *Catal. Sci. Technol.* **2015**, *5*, 5048−5061.
(38) Ye, S.; Wang, R.; Wu, M. Z.; Yuan, Y. P. A review on g-C_3N_4 for photocatalytic water splitting and CO_2 reduction. *Appl. Surf. Sci.* **2015**, *358*, 15−27.
(39) Martin, D. J.; Qiu, K.; Shevlin, S. A.; Handoko, A. D.; Chen, X.; Guo, Z.; Tang, J. Highly Efficient Photocatalytic H_2 Evolution from Water using Visible Light and Structure-Controlled Graphitic Carbon Nitride. *Angew. Chem., Int. Ed.* **2014**, *53*, 9240−9245.
(40) Kang, Y.; Yang, Y.; Yin, L. C.; Kang, X.; Liu, G.; Cheng, H. M. An Amorphous Carbon Nitride Photocatalyst with Greatly Extended Visible-Light-Responsive Range for Photocatalytic Hydrogen Generation. *Adv. Mater.* **2015**, *27*, 4572−4577.
(41) Han, Q.; Wang, B.; Zhao, Y.; Hu, C.; Qu, L. A Graphitic-C_3N_4 "Seaweed" Architecture for Enhanced Hydrogen Evolution. *Angew. Chem., Int. Ed.* **2015**, *54*, 11433−11437.
(42) Li, X.; Bi, W.; Zhang, L.; Tao, S.; Chu, W.; Zhang, Q.; Luo, Y.; Wu, C.; Xie, Y. Single-Atom Pt as Co-Catalyst for Enhanced Photocatalytic H_2 Evolution. *Adv. Mater.* **2016**, *28*, 2427−2431.
(43) Xu, J.; Li, Y.; Peng, S.; Lu, G.; Li, S. Eosin Y-sensitized graphitic carbon nitride fabricated by heating urea for visible light photocatalytic hydrogen evolution: the effect of the pyrolysis temperature of urea. *Phys. Chem. Chem. Phys.* **2013**, *15*, 7657−7665.
(44) Zhao, H.; Dong, Y.; Jiang, P.; Miao, H.; Wang, G.; Zhang, J. In situ light-assisted preparation of MoS_2 on graphitic C_3N_4 nanosheets for enhanced photocatalytic H 2 production from water. *J. Mater. Chem. A* **2015**, *3*, 7375−7381.
(45) Kong, L.; Dong, Y.; Jiang, P.; Wang, G. L.; Zhang, H.; Zhao, N. Light-assisted rapid preparation of Ni/g-C_3N_4 magnetic composite for robust photocatalytic H_2 evolution from water. *J. Mater. Chem. A* **2016**, *4*, 9998−10007.

DOI: 10.1021/acssuschemeng.7b01079
ACS Sustainable Chem. Eng. 2017, 5, 6845−6853

(46) Yan, H.; Chen, Y.; Xu, S. Synthesis of graphitic carbon nitride by directly heating sulfuric acid treated melamine for enhanced photocatalytic H_2 production from water under visible light. *Int. J. Hydrogen Energy* **2012**, *37*, 125−133.
(47) Pu, Z.; Liu, Q.; Tang, C.; Asiri, A. M.; Sun, X. Ni_2P nanoparticle films supported on a Ti plate as an efficient hydrogen evolution cathode. *Nanoscale* **2014**, *6*, 11031−11034.
(48) Zhang, X.; Xie, X.; Wang, H.; Zhang, J.; Pan, B.; Xie, Y. Enhanced photoresponsive ultrathin graphitic-phase C_3N_4 nanosheets for bioimaging. *J. Am. Chem. Soc.* **2013**, *135*, 18−21.
(49) Menezes, P. W.; Indra, A.; Das, C.; Walter, C.; Goebel, C.; Gutkin, V.; Schmeißer, D.; Driess, M. Uncovering the nature of active species of nickel phosphide catalysts in high-performance electrochemical overall water splitting[J]. *ACS Catal.* **2017**, *7*, 103−109.
(50) Cao, S.; Low, J.; Yu, J.; Jaroniec, M. Polymeric photocatalysts based on graphitic carbon nitride. *Adv. Mater.* **2015**, *27*, 2150−2176.

DOI: 10.1021/acssuschemeng.7b01079
ACS Sustainable Chem. Eng. 2017, 5, 6845−6853